Chapter 6
Electrochemically Produced Metal Powders

6.1 Introduction

Powders are finely divided solids, smaller than 1000 μm in its maximum dimension. A particle is defined as the smallest unit of a powder. The particles of powder may assume various forms and sizes, whereas the powders, as an association of such particles, exhibit, more or less, the same characteristics as if they were formed under identical conditions and if the manipulation of the deposits after removal from the electrode was the same [1, 2]. The size of particles of many metal powders can vary in a quite wide range from a few nanometers to several hundreds of micrometers. The most important properties of a metal powder are the specific surface, the apparent density, the flowability, and the particle grain size distribution. These properties, called decisive properties, characterize the behavior of a metal powder.

Different methods for the production of metal powders including mechanical commuting, chemical reaction, electrolysis, and liquid metal atomization are used in practice [1]. Powders of about 60 metals can successfully be produced by electrolysis. The majority of metallic powders are obtained by molten salt electrolysis. However, due to technological advantages and various industrial applications, most of the practically useful powders, *e.g.*, copper, iron, nickel, *etc.*, are produced from aqueous solutions [3]. Formation of powders by electrolysis is an economical processing method with a low capital investment and operational cost. The main advantages of this method in relation to other methods of powder production are high purity of the produced powder which can be easily pressed and sintered and low oxygen content [1, 2]. It has environmentally friendly way of powder production which enables working in a closed circuit [4].

Dendrites are the most common shape of electrochemically produced powder particles [5]. Aside from dendrites, powder particles can be also obtained in the form of flakes, fibrous, spongy, wires, cauliflower-like, and the many other irregular forms. The powder particles can spontaneously fall off or can be removed from the

K.I. Popov et al., *Morphology of Electrochemically and Chemically Deposited Metals*, DOI 10.1007/978-3-319-26073-0_6

electrode by tapping or other similar techniques. In this chapter, all these electrodeposited forms before their removal from the electrode surface are also treated as powder particles.

Metal powders can be formed by both potentiostatic and galvanostatic regimes of electrolysis [2, 5–7]. In the galvanostatic regime of electrolysis, all metals which can be electrodeposited exhibit a tendency to appear in the form of powders at current densities larger than a certain critical value which is equal to the limiting diffusion current density [7, 8]. In the potentiostatic regime of electrolysis, metals are electrodeposited in the powder form at overpotentials inside the plateau of the limiting diffusion current density, as well as at the higher ones [7]. In addition, metal powders can be produced under periodically changing regimes of electrolysis, such as pulsating overpotential (PO), pulsating current (PC), and reversing current (RC) [5–7]. Application of electrodeposition at a periodically changing rate offers a great possibility in the electrochemical production of metal powders.

6.2 Morphology of Powder Particles in the Dependence of the Exchange Current Density and Hydrogen Overpotential

The shape of electrochemically formed powder particles strongly depends on the electrodeposition conditions, such as the electrolysis regime, the composition of solution, the type of the working electrode, and the temperature and the nature of the metal. Regarding the values of the exchange current density, i_0, and melting points, T_m, metals are classified into three classes [9, 10]:

(a) *Class I, so-called normal metals*: Pb, Sn, Tl, Cd, Hg, Zn, Ag (simple electrolytes). These metals are characterized by low T_m and high i_0 ($i_0 > 1$ A dm^{-2}) values. Additionally, they show high overpotentials for hydrogen discharge.

(b) *Class II, intermediate metals*: Cu, Au, Ag (complex electrolytes). These metals are characterized by moderate T_m, medium i_0 (i_0 in the interval from 10^{-2} to 1 A dm^{-2}), and lower hydrogen overpotentials.

(c) *Class III, inert metals*: Fe, Co, Ni, Mn, Cr, Pt. These metals have high T_m, low i_0, and very low hydrogen overpotentials. For this class of metals, i_0 is between 10^{-2} and 10^{-12} A dm^{-2}.

6.2.1 Class I: So-Called Normal Metals

Due to the high exchange current density values, i_0, the processes of electrodeposition of the normal metals belong to the fast electrochemical processes which enable formation of powder at the relatively low overpotentials [5]. The dendrites of normal metals are mainly 2D (two dimensional), and the shape of the dendrites of

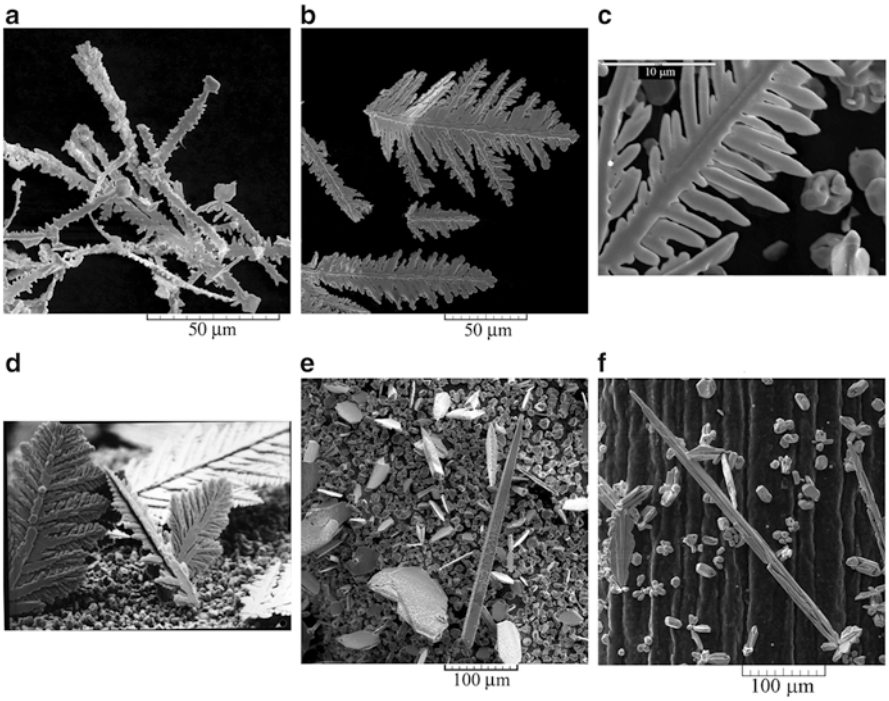

Fig. 6.1 Pb, Ag, and Cd powders electrodeposited from (**a**) Pb; 0.10 M $Pb(NO_3)_2 + 2.0$ M $NaNO_3$; overpotential, $\eta = 100$ mV, (**b**) Pb; 0.10 M $Pb(CH_3COO)_2 + 1.5$ M $NaCH_3COO + 0.15$ M CH_3COOH; $\eta = 100$ mV, (**c**) Ag; 0.060 M $AgNO_3 + 1.2$ M $NaNO_3 + 0.050$ M HNO_3; $\eta = 150$ mV, (**d**) Cd; 0.10 M $CdSO_4 + 0.50$ M H_2SO_4; $\eta = 110$ mV, × 400, (**e**) Pb; 0.30 M $Pb(NO_3)_2 + 2.0$ M $NaNO_3$; $\eta = 55$ mV, and (**f**) Ag; 0.10 M $AgNO_3 + 2.0$ M $NaNO_3$; $\eta = 100$ mV (Reprinted from Refs. [11–13] with kind permission from Springer, Ref. [14] with permission from Elsevier and Ref. [15] with permission from Electrochemical Society)

this group of metals follows the classical Wranglen definition of a dendrite (Fig. 6.1). According to Wranglen [16], a dendrite is a skeleton of a monocrystal and consists of a stalk and branches, thereby resembling a tree. The dendrite consisted only of the stalk, and primary branches is referred as primary (P) dendrite. If the primary branches in turn develop secondary branches, the dendrite is called secondary (S). The two-dimensional (2D) dendrite refers to dendrites with branches that lie in the same plane as that of the primary stalk [17].

The shape of dendrites depends not only on the nature of metals but also on the type of used electrolyte. For example, the 2D Pb dendrites of the P type are obtained from the basic (nitrate) electrolyte (Fig. 6.1a), while the 2D Pb dendrites of the S type are obtained from the complex (acetate) electrolyte (Fig. 6.1b) [11, 14, 18]. As far as the shape of dendrites of the other metals from this group, they also belong to either P (Ag; Fig. 6.1c) [12, 15] or S (Cd; Fig. 6.1d) types [5, 12, 13, 19]. The branchy Pb and Cd dendrites of the S type are usually referred as the fern-like ones [13, 14]. Aside from the (P) and (S) dendrites, these metals are also electrodeposited

in the needle-like form (Fig. 6.1e, f). The appearance of tertiary branches in branchy Pb dendrites is also possible [11].

In contrast to the very different morphology of the Pb powder particles obtained from the different electrolytes, the crystallographic structure of powder particles does not depend on the type of electrolyte [11, 18]. Irrespective of the type of electrolytes, the dominant presence of Pb crystallites oriented in the (111) plane was observed in the powder particles obtained from both basic and complex electrolytes.

6.2.2 *Class II: Intermediate Metals*

The shape of dendrites of the group of the intermediate metals is completely different from those of the group of the normal metals. They are the 3D (three dimensional) pine-like constructed from a long trunk or stem with corncob-like branches oriented in all directions (Fig. 6.2a–c) [7, 12, 15, 20]. There is no any difference in the shape of dendrites among metals from this group (Fig. 6.2a, c – Ag (ammonium electrolyte) and Fig. 6.2b – Cu). The similar shape of dendrites is also obtained by the processes of electrodeposition of Au [21] and Ag from the other types of complex electrolytes (*i.e.*, in the presence of tungstosilicate [22] and citric [23] acids). This similarity in the form of dendrites at the macrolevel clearly indicates that the pine-like shape of dendrites represents the typical form of a dendrite characterizing the group of intermediate metals.

The corncob-like forms were mutually parallel and oriented at an approximate angle of about 60° in relation to the stalk or trunk, indicating the existence of high structural symmetry of this group of dendrites. The corncob-like forms were constructed from small agglomerates of metal grains indicating on the similarity the pine-like dendrites, not only on the macro- but also on the microlevel. The treatment of copper dendrites using ultrasound [24, 25] showed that the corncob-like forms represent the basic element of which these dendrites were constructed.

The pine-like Ag and Cu dendrites shown in Fig. 6.2a, b were electrodeposited inside the plateaus of the limiting diffusion current density [20]. The Ag dendrites were also formed outside the plateau of the limiting diffusion current density in the zone of a sharp increase in the current density with an increase in the overpotential (Fig. 6.2c).

However, due to the fact that hydrogen evolution reaction on copper electrode is somewhat faster than on silver electrode (in the case of Ag, there is no hydrogen evolution even at an overpotential of 1000 mV *vs*. Ag reference electrode) [15, 20], hydrogen evolution as a parallel reaction to Cu electrodeposition at high overpotentials commencing at the overpotential inside the plateau of the limiting diffusion current density causes an inhibition of dendritic growth. In the dependence of concentration of Cu^{2+} ions, the honeycomb-like structures are usually formed outside the plateau of the limiting diffusion current density (Fig. 6.2d), and the particles of cauliflower-like shape are obtained after a removal of deposits from

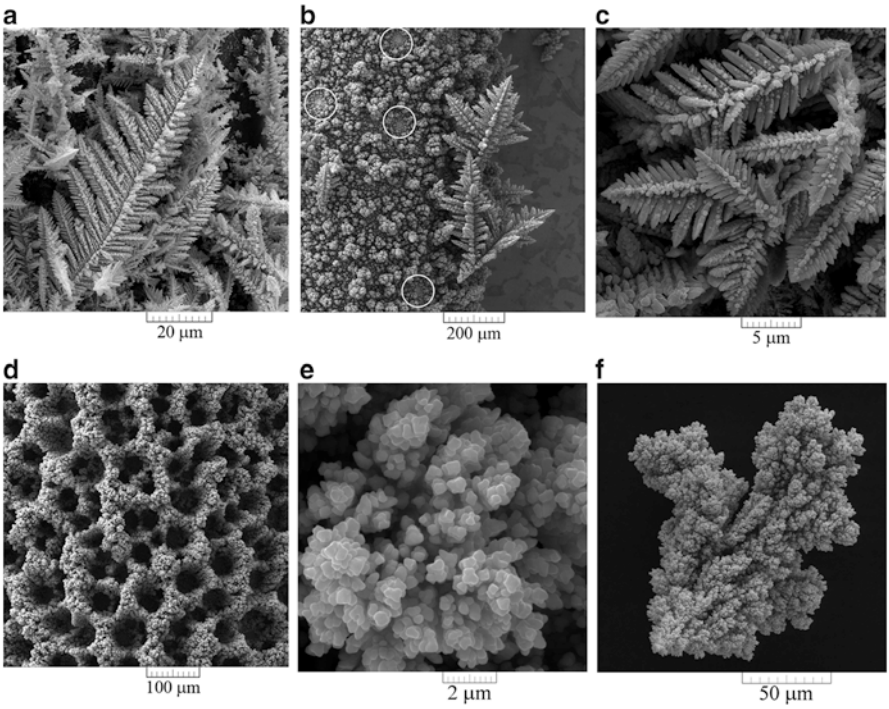

Fig. 6.2 Ag and Cu powders electrodeposited from (**a**) Ag; 0.10 M $AgNO_3 + 0.50$ M $(NH_4)_2SO_4 + NH_4OH$ to dissolve the silver sulfate precipitate; $\eta = 650$ mV, (**b**) Cu; 0.10 M $CuSO_4 + 0.50$ M H_2SO_4; $\eta = 650$ mV, part in circles: holes formed of detached hydrogen bubbles, (**c**) Ag; 0.10 M $AgNO_3 + 0.50$ M $(NH_4)_2SO_4 + NH_4OH$ to dissolve the silver sulfate precipitate; $\eta = 1000$ mV, (**d**–**f**) Cu; 0.10 M $CuSO_4 + 0.50$ M H_2SO_4; $\eta = 1000$ mV (Reprinted from Ref. [20] with permission from Society of Chemists and Technologists of Macedonia)

them (Fig. 6.2e, f). The cauliflower-like particles were constructed from small agglomerates of Cu grains, indicating on the similarity of microstructure of these particles with dendritic ones [7].

6.2.3 Class III: Inert Metals

Due to the low overpotentials for hydrogen evolution reaction for metals from this group, electrodeposition of inert metals occurs parallel with hydrogen evolution reaction in the whole range of current densities and potentials. Dendritic growth is mainly inhibited by generated hydrogen, and the spongy-like, cauliflower-like, and globular particles, very similar to each other, were predominately formed by electrodepositions of Co, Ni, and Fe (Fig. 6.3a–c) [12, 26, 27, 29, 30]. The shape of 3D fern-like dendrites was strongly affected by generated hydrogen, and the

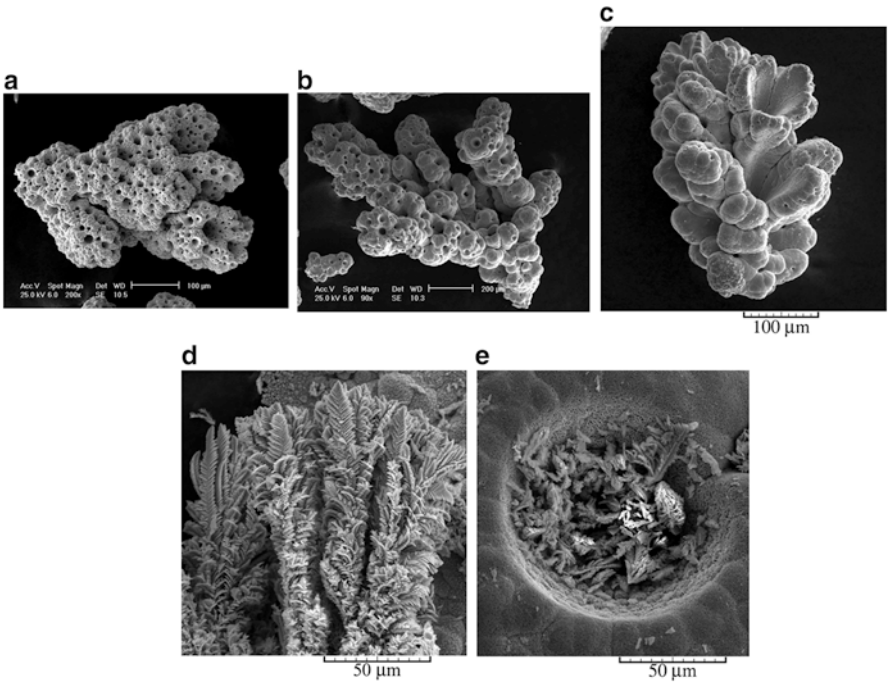

Fig. 6.3 Ni, Co, and Fe powders electrodeposited from (**a**) Ni: 0.10 M $NiCl_2 + 1.0$ M $NH_4Cl + 0.70$ M NH_4OH under the condition of limiting current density, (**b**) Co: 0.10 M $CoCl_2 + 1.0$ M $NH_4Cl + 0.70$ M NH_4OH under the condition of limiting current density, (**c**) Fe: 1.0 M $NH_4Cl + 0.20$ M $Na_3C_6H_5O_7 + 0.10$ M $FeCl_2$, pH = 4.0, (**d**, **e**) Co: 0.10 M $CoSO_4 + 0.70$ M $NH_4OH + 1.0$ M $(NH_4)_2SO_4$; $i = 500$ mA cm^{-2} (Reprinted from Ref. [12] with kind permission from Springer, Refs. [26, 27] with permission from Elsevier, and Ref. [28] with permission from the Serbian Chemical Society)

dendrites are formed at the lower current densities, as well as in the interior of holes where there is no the effect of evolved hydrogen on a solution stirring in the near-electrode layer (Fig. 6.3d, e) [28].

6.3 The Characteristics of Electrochemically Produced Powder: A General Discussion

Comparative survey of powders obtained in potentiostatic and galvanostatic regimes of electrolysis is shown in Fig. 6.4. In spite of the fact that particles obtained by galvanostatic deposition are less dendritic than those obtained by potentiostatic deposition due to smaller overpotential at the end of the galvanostatic than the potentiostatic regimes [5], there is no any substantial difference in the morphology of powder particles obtained between these two constant regimes of

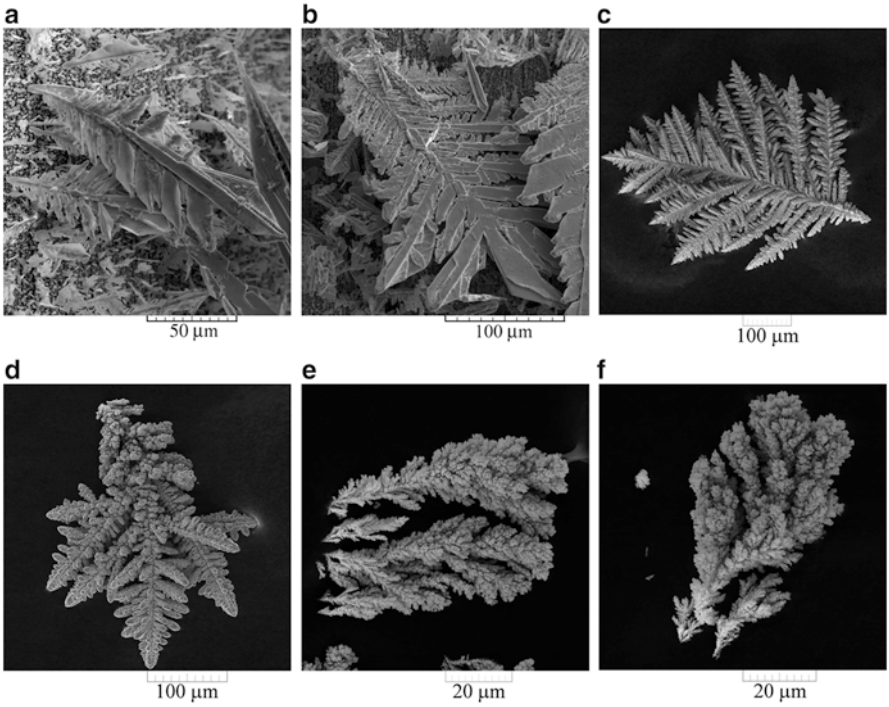

Fig. 6.4 Pb particles electrodeposited from 0.50 M $Pb(NO_3)_2 + 2.0$ M $NaNO_3$: (**a**) the potentiostatic regime: $\eta = 150$ mV, (**b**) the galvanostatic (DC) regime: $i = 160$ mA cm^{-2}, and Cu particles electrodeposited from 0.10 M $CuSO_4 + 0.50$ M H_2SO_4: (**c**) $\eta = 650$ mV, (**d**) $i = 16$ mA cm^{-2}, (**e**) $\eta = 1000$ mV, and (**f**) $i = 440$ mA cm^{-2} (Reprinted from Refs. [12, 31] with kind permission from Springer)

electrolysis (Pb powder (Fig. 6.4a – the potentiostatic regime and Fig. 6.4b – the galvanostatic regime) and Cu powder (Fig. 6.4c, e – the potentiostatic regime and Fig. 6.4d, f – the galvanostatic regime)).

As previously mentioned, the shape of powder particles depends on both the exchange current density and hydrogen evolution reaction. The lowering of the exchange current density causes a branching of dendrites and their transformation from the 2D into 3D ones. The range of overpotentials corresponding to electrodeposition of metals in the powder form is shifted toward the higher overpotentials, and the increase of the diffusion part at the polarization curve was observed with the decrease of the exchange current density.

The process of complex formation also decreases the exchange current density causing both the increase of the diffusion part and the branching of dendrites [14]. Comparative analysis of the polarization and morphological characteristics of lead for the basic (nitrate) and complex (acetate) electrolytes is presented in Fig. 6.5. In the case of silver, this lowering of the exchange current density is so strong to cause transfer of Ag from the group of normal ($i_0 \to \infty$ for the nitrate

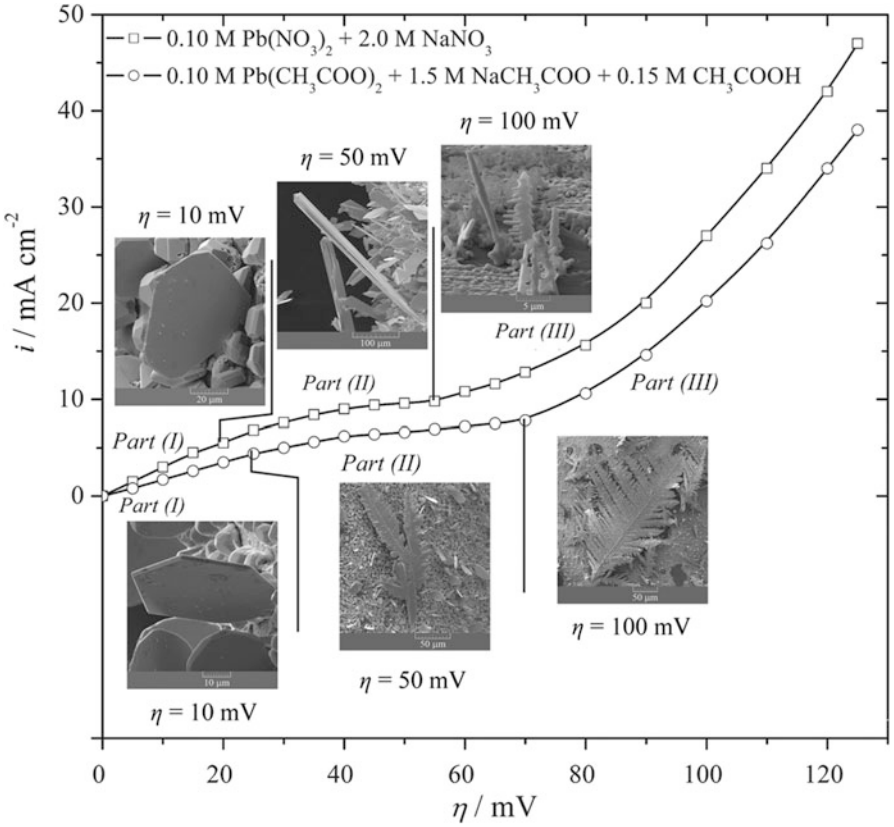

Fig. 6.5 The comparative survey of the polarization curves and the typical morphologies of lead deposits electrodeposited from 0.10 M $Pb(NO_3)_2 + 2.0$ M $NaNO_3$ and 0.10 M Pb $(CH_3COO)_2 + 1.5$ M $NaCH_3COO + 0.15$ M CH_3COOH (Reprinted from Ref. [11] with kind permission from Springer and Ref. [14] with permission from Elsevier)

electrolytes; Fig. 6.1c, f) to the group of intermediate metals ($i_0 \ll i_L$ for the ammonium electrolyte; Fig. 6.2a, c).

The second factor which strongly affects morphology of powder particles is hydrogen evolution reaction as parallel reaction to metal electrodeposition. The effect of this parallel reaction already becomes visible during electrodeposition of Cu at the high overpotentials (Fig. 6.2d–f), and evolution of hydrogen just defines the transitional character of the intermediate metals between the normal and the inert metals. Thanks to this reaction, the same shape of the polarization curves for ammonium Ag (the high hydrogen overpotential for hydrogen evolution reaction) and Cu (the lower hydrogen evolution overpotential than for Ag) gives a completely different morphology of Ag and Cu powders in the zone of fast increase of the current density with increasing the overpotential (Fig. 6.6).

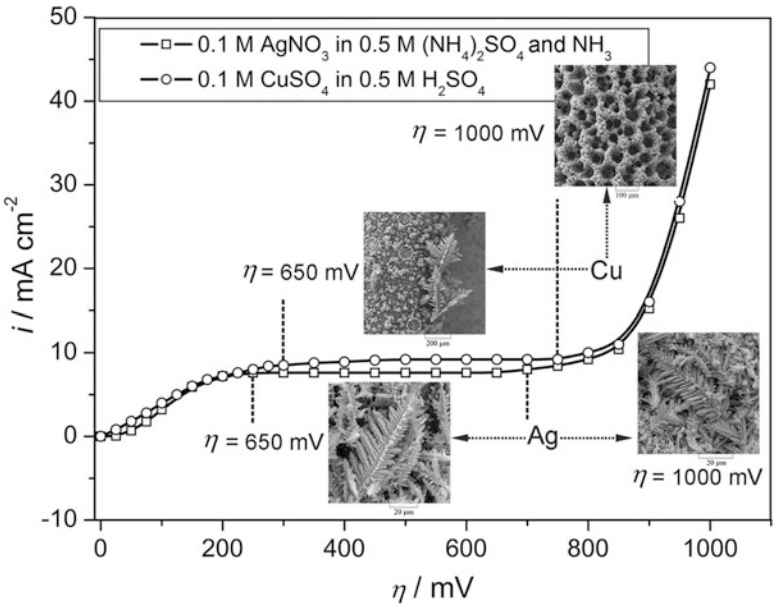

Fig. 6.6 Comparative survey of the polarization and morphological characteristics of Cu and Ag (Reprinted from Ref. [20] with permission from Society of Chemists and Technologists of Macedonia)

Due to the ionic equilibrium of the species in the $CuSO_4$-H_2SO_4-H_2O system (the most often employed electrolytes for the electrodeposition of copper are sulfate ones), the shape of powder particles depends on $CuSO_4$ and H_2SO_4 concentrations [32–34]. For a constant H_2SO_4 concentration, the H^+ ion concentration decreases with increasing Cu^{2+} concentration that is manifested by the change of shape of powder particles from the cauliflower-like to dendritic ones.

Of course, hydrogen evolution affects mechanism of formation of powder particles. The dendrites are formed without, as well as with, a quantity of evolved hydrogen (the case of Cu) which was insufficient to achieve any effect on the hydrodynamic conditions in the near-electrode layer. Then, the electrodeposition process was primarily controlled by the diffusion of ions to the electrode surface, rather than the kinetic of the electrodeposition [5, 6]. The cauliflower-like particles are formed in the conditions of vigorous hydrogen evolution with the strong effect of evolved hydrogen on the hydrodynamic conditions in the near-electrode layer, and the concept of "effective overpotential" is proposed to explain formation of these particles [25, 35].

Finally, hydrogen evolution becomes crucial factor determining the shape of powder particles of the group of the inert metals, and the concept of "effective overpotential" is applicable to explain the formation of these powder particles. Due to vigorous hydrogen evolution, dendritic growth is almost completely inhibited. Analysis of the polarization curves for Co and Ni [12, 26, 30] showed that their

shape is a consequence of the so-called electrode effect which is connected to the bubble formation at high current densities; as a result, the evolution of bubbles became the rate-limiting step of the electrochemical process. The current for hydrogen evolution at more negative potentials reached 60–70 % of the total current.

6.4 Application of Periodically Changing Regimes of Electrolysis on Formation of Metal Powders

Powder particles with different grain size and morphology can be obtained by varying the wave of periodically changing current or overpotential [6]. In the dependence of the shape of square-wave pulsating overpotential (PO), it can be obtained either dendritic (Fig. 6.7a) or cauliflower-like (Fig. 6.7b) Cu particles [36]. Please note that both particles are obtained with same overpotential amplitude of 1000 mV. The applied parameters of the PO regime have influence on both hydrogen evolution reaction and metal electrodeposition rate. Generally, application of square-wave PO with deposition pulses, t_c, shorter than pause durations, t_p, suppresses the hydrogen evolution reaction and favors the growth of dendrites, while the applied square-wave PO with t_c longer than t_p favors formation of cauliflower-like particles. In this way, the effect of shortening of deposition pulse is equivalent to the decrease of the overpotential of electrodeposition in the potentiostatic regime of electrolysis. It is clear that dendrite obtained by the PO regime (Fig. 6.7a) is very similar to the one obtained at a constant overpotential of 650 mV (Fig. 6.2b). On the other hand, morphology of cauliflower-like particle shown in Fig. 6.7b approaches to the one obtained at an overpotential of 1000 mV (Fig. 6.2d).

The similar consideration is also valid for the regime of pulsating current (PC) [37]. The branchy dendrites are formed with deposition pulses, t_c, shorter than pause duration, t_p, (Fig. 6.7c), and cauliflower-like particles are formed with t_c longer than t_p (Fig. 6.7d). Effects attained by the choice of appropriate parameters of square-wave PC were equivalent to those obtained by electrodeposition at the constant overpotential from solutions of different concentrations of $CuSO_4$ and H_2SO_4. Increasing concentration of Cu^{2+} ions was equivalent to the effect of the decreasing deposition pulses, while the constant pause duration was equivalent to H_2SO_4 concentration used. The effect of increasing H_2SO_4 concentration was equivalent to the effect to the decreasing pause duration, while the constant $CuSO_4$ concentration is equivalent to the constant deposition pulse used [37]. Simultaneously, the constant overpotential used corresponds to the amplitude current density used.

The periodically changing regimes also affect strongly the shape of powder particles of metals with high overpotentials for hydrogen discharge (*Class I*). Unlike of the fern-like dendrites obtained at the constant overpotential

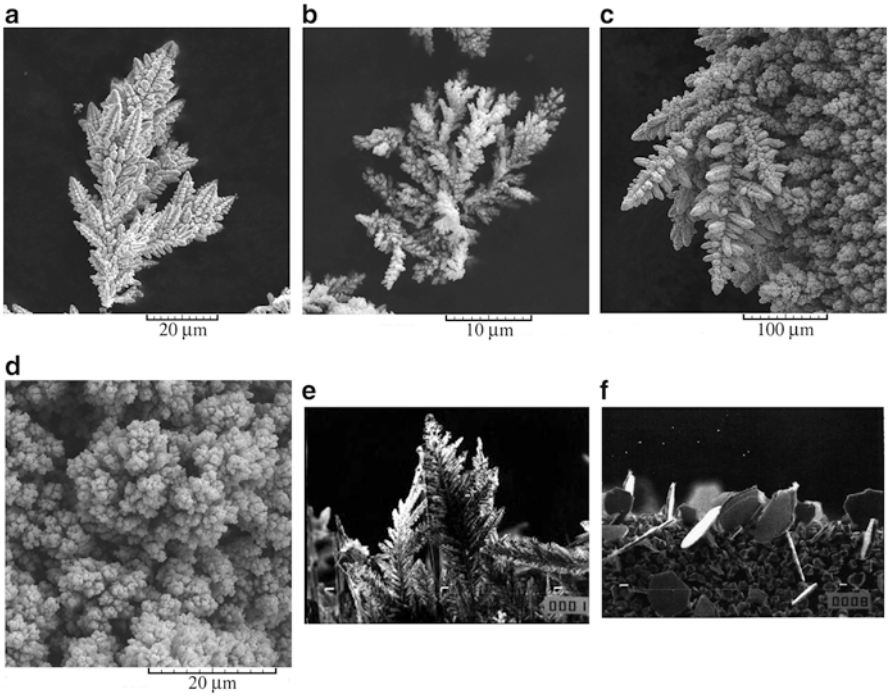

Fig. 6.7 Cu particles electrodeposited from 0.15 M $CuSO_4$ in 0.50 M H_2SO_4 by the regime of (**a**) pulsating overpotential (PO); the overpotential amplitude, η_A: 1000 mV; pause duration, t_p: 10 ms; deposition pulse, t_c: 3 ms, (**b**) PO; η_A: 1000 mV; t_p: 10 ms; t_c: 20 ms, (**c**) pulsating current (PC); the current density amplitude, i_A: 0.20 A cm^{-2}; t_p: 10 ms; t_c: 1 ms, (**d**) PC; i_A: 0.20 A cm^{-2}; t_p: 10 ms; t_c: 50 ms, and Pb particles obtained from 0.10 M $Pb(CH_3COO)_2 + 1.5$ M $NaCH_3COO + 0.15$ M CH_3COOH: (**e**) the constant overpotential: 75 mV; $t = 50$ s; × 500, and (**f**) PO; η_A: 75 mV; t_c: 0.1 ms; pause to pulse ratio: 3; × 1000 (Reprinted from Ref. [7] with kind permission from Springer and Refs. [36–38] with permission from Elsevier)

(Fig. 6.7e), Pb particles of irregular shape (denoted as irregular crystals or precursors of dendrites) (Fig. 6.7f) were obtained by the appropriate square-wave PO with the overpotential amplitude equal to the overpotential of electrodeposition in the constant potentiostatic regime of electrolysis [5, 38]. As a remainder, in the constant potentiostatic regimes of electrolysis, irregular crystals are formed at lower overpotentials than the fern-like dendrites.

6.5 Analysis of Decisive Properties of Powders and Their Mutual Relations

The properties of metal powder, denoted as the decisive properties, characterize the behavior of metal powders. The most important of them are the specific surface, the apparent density, the flowability, the particle grain size, and the particle size

distribution [1]. These properties were analyzed by Popov et al. [39–54] for Cu powder that is taken as a model system. It is shown that some of properties of Cu powders can be mutually related, as well as that the specific surface of copper powder can be related to overpotential of electrodeposition [39, 40]. In this way, correlation between properties of metal powders and conditions of electrodeposition was enabled.

6.5.1 *Correlation Between Specific Surface and Overpotential of Electrodeposition*

The specific surface of a powder and a powdered deposit is determined as the surface per unit of the mass of powder.

It is well known [55, 56] that the surface coarseness during potentiostatic electrodeposition in the mixed activation–diffusion control increases with the increase of the current density of electrodeposition. The surface coarseness also increases during potentiostatic electrodeposition at the limiting diffusion current density with an increase of overpotential [57, 58], resulting in the formation of dendrites. In metal electrodeposition in the limiting diffusion current density range, the real current density remains constant regardless of overpotential used. Simultaneously, the larger overpotential of electrodeposition is used, the more disperse deposit characterized by the increased specific surface is formed.

The last effect can be qualitatively discussed as follows. In the Eq. (1.31), the activation part of electrodeposition overpotential required for the charge transfer, η_{act}, is given by Eq. (2.89), while the rest of the overpotential is due to mass transfer limitations, η_{diff}, given by Eq. (6.1):

$$\eta_{diff} = \frac{b_c}{2.3} \ln \frac{1}{1 - \frac{i}{i_L}} \tag{6.1}$$

Hence, if $i \to i_L$,

$$\eta_{act} = \frac{b_c}{2.3} \ln \frac{i_L}{i_0} \tag{6.2}$$

being equal to the critical overpotential for the initiation of dendritic growth [5, 59]. Simultaneously, for $i \to i_L$

$$\eta_{diff} \to \infty \tag{6.3}$$

It is obvious that a very small increase of current density in the limiting diffusion current density range causes a large increase in deposition overpotential. Hence, the charge transfer overpotential and the ohmic drop in the solution remain the same for all overpotentials belonging to the limiting diffusion current density plateau,

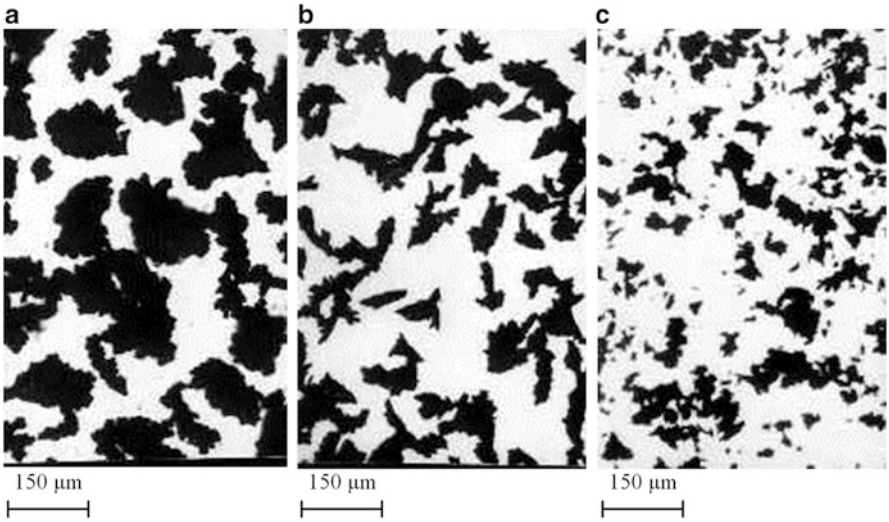

Fig. 6.8 Copper powder particles obtained at different overpotentials from 0.10 M $CuSO_4$ in 0.50 M H_2SO_4 onto stationary platinum wire electrodes painted with shellac. Deposition time: 15 min. Overpotentials of electrodeposition: (**a**) 500 mV, (**b**) 600 mV, and (**c**) 700 mV (Reprinted from Ref. [5] with kind permission from Springer)

regardless of electrodeposition overpotential. This is due to the fact that both the charge transfer overpotential and the ohmic drop only depend on the current density. On the other hand, an increase of the deposition overpotential in the limiting diffusion current density range causes a strong increase of the dispersity, as illustrated by Fig. 6.8, and leads to an increase of the specific surface area of metal deposits. Hence, it seems reasonable to assume that the difference in overpotential of electrodeposition can be related to the increase of the surface of the deposited metal by Eq. (6.4) [39, 40]:

$$\gamma_s(S_2 - S_1) = (\eta_2 - \eta_1)\int_0^t I\mathrm{d}t \tag{6.4}$$

where I is a current of electrodeposition, t is a time of electrodeposition, $\int_0^t I\mathrm{d}t$ is the quantity of passed electricity, η_2 and η_1 are overpotentials of electrodeposition belonging to the limiting diffusion current density range, S_2 and S_1 are the surface area of disperse deposits at the overpotentials η_2 and η_1, respectively, and γ_s is the surface energy of disperse deposit formation.

Equation (6.4) can be rewritten in the form:

$$\gamma_s = \frac{(\eta_2 - \eta_1)\int_0^t I\mathrm{d}t}{(S_2 - S_1)} \tag{6.5}$$

for the direct determination of the energy of disperse solid copper surface formation in sulfate solutions.

The energy of disperse solid copper surface formation, γ_s, calculated by Eq. (6.5) includes all energetic loses during electrodeposition in the range of the limiting diffusion current densities.

For the estimation of the surface energy of disperse deposits formation, γ_s, according to Eq. (6.5), it is necessary to determine surface area of deposits, S_2 and S_1, at overpotentials η_2 and η_1 belonging to the limiting diffusion current density range. Obviously, the surface area of a deposit, S_1, corresponds to an overpotential η_1 at the beginning of the limiting diffusion current density plateau, while the surface area of a deposit, S_2, corresponds to an overpotential η_2 at the end of the limiting diffusion current density plateau. During the depositions, $I - t$ dependences were recorded and the quantity of electricity, $\int_0^t I\mathrm{d}t$ was determined by a graphical integration.

Due to very high surface areas of powdered (or disperse) deposits, the determination of real surface area of this deposit type can represent serious problem [52]. The determination of the real surface area of disperse metal deposits by some common methods, such as the use of STM and AFM techniques (using the option *surface area diff.*, in the accompanying software package), is not possible, because these techniques are only suitable for the determination of the real surface area of compact and relatively smooth surface area [60]. For that reason, the new and relatively easy way for the estimation of the real surface area of disperse deposits was proposed by Popov et al. [39, 40, 52]. For copper solution containing 0.15 M $CuSO_4$ in 0.50 M H_2SO_4, this estimation can be presented in the following way: working electrode (copper or platinum of the surface area $S_{0,i}$) is covered by a thin copper film by electrodeposition at an overpotential of 300 mV during 2 min. After a relaxation of the diffusion layer for 15 min, current at an overpotential of 50 mV, I_0, is recorded, being proportional to the original electrode surface area $S_{0,i}$. The overpotential is then adjusted to the desired value and electrodeposition is carried out. After the determined quantity of electricity had been reached, the overpotential is decreased to 50 mV, and after relaxation of the diffusion layer for 15 min, the current, I_η, corresponding to the surface area S_f generated during electrodeposition, is determined. The surface area of the deposit is then calculated using the Eq. (6.6):

$$S_f = S_{0,i}\frac{I_\eta}{I_0} - S_{0,i} = S_{0,i}\left(\frac{I_\eta}{I_0} - 1\right) \tag{6.6}$$

It is well known [57] that dendrites are not formed at overpotentials of electrodeposition lower than a critical overpotential for dendritic growth initiation, η_i, and that powdered deposits characterized by a very large surface area are formed at overpotentials higher than some critical value, η_c.

For $\eta_2 \geq \eta_c$, $\eta_1 \geq \eta_i$, and $S_2 \gg S_1$, Eq. (6.5) can be rewritten in the form:

$$S_2 = \frac{(\eta_2 - \eta_1)\int_0^t I\mathrm{d}t}{\gamma_s} \tag{6.7}$$

On the other hand, the quantity of electrodeposited metal m_{sp} is given by:

$$m_{sp} = \frac{M}{nF}\int_0^t I\mathrm{d}t \tag{6.8}$$

assuming the current efficiency for metal electrodeposition, $\eta_I(M)$ to be 1, and M is the atomic mass of deposited metal. From Eqs. (6.7) and (6.8), the specific powder (or powdered deposit) surface S_{sp} is:

$$S_{sp} = \frac{S_2}{m} = \frac{(\eta_2 - \eta_1)nF}{\gamma_s M} \tag{6.9}$$

If the current efficiency for metal electrodeposition, $\eta_I(M)$, is lower than 1, Eq. (6.8) becomes:

$$m_{sp} = \eta_I(M)\frac{M}{nF}\int_0^t I\mathrm{d}t \tag{6.10}$$

and Eq. (6.9) becomes:

$$S_{sp} = \frac{(\eta_2 - \eta_1)nF}{\eta_I(M)\gamma_s M} \tag{6.11}$$

Equations (6.10) and (6.11) are valid in the hydrogen evolution range at overpotentials lower than the critical one for the change of the growth of dendrites. The situation is dramatically different in galvanostatic electrodeposition of powder. In this case, due to the increase of the surface coarseness, the low increase of the limiting diffusion current density caused by the increase of the surface area of a

deposit leads to the strong decrease of overpotential of the electrodeposition in the limiting diffusion current density range even with the short deposition times. The internal structure of powder particles is not changed with a time during potentiostatic electrodeposition, and it only depends on the presence or the absence of hydrogen evolution. In the galvanostatic case, the structure of particles becomes more compact with the increasing time of electrodeposition, and it can be changed from dendrites at the beginning of the electrodeposition process to the compact one with the longer electrodeposition time, as shown in Fig. 6.9a, b [41, 47, 50]. In the hydrogen evolution range, overpotential of electrodeposition is determined by the hydrogen reduction and at the sufficiently large initial current densities, $i \gg i_L$, as well as with enough short electrodeposition times, formation of copper powder in a galvanostatic deposition becomes similar to the one in potentiostatic electrodeposition, as shown in Fig. 6.9c, d.

The described method for the determination of the specific surface of electrodeposited copper is applicable if some kind of a Faradaic cage is not formed on the surface of deposit, *i.e.*, when the formed structure is "open" to the bulk of electrolyte solution in potentiostatic deposition.

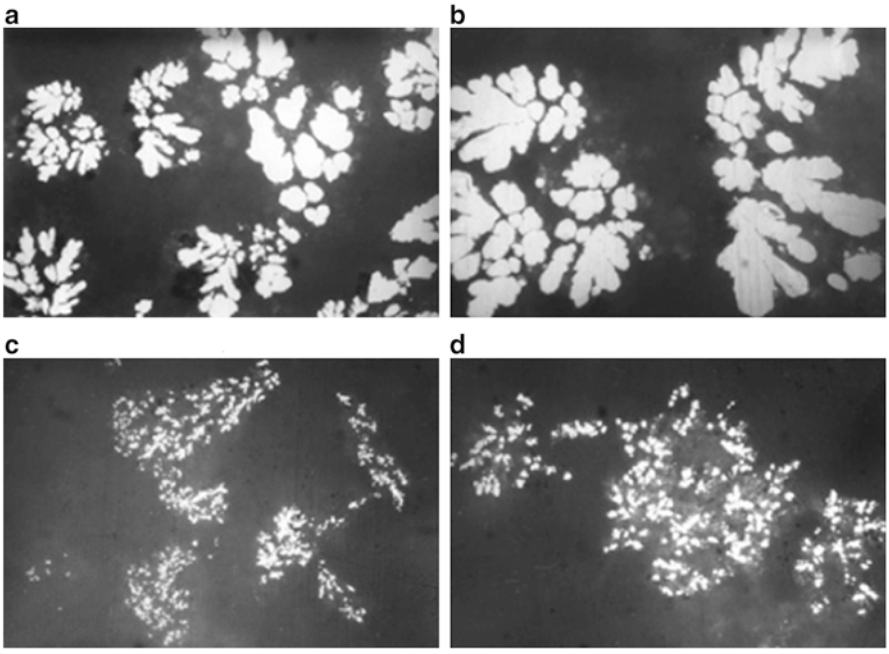

Fig. 6.9 SEM photomicrographs of copper powder particles obtained in constant current deposition. $c(Cu^{2+}) = 15$ g dm^{-3}; $c(H_2SO_4) = 140$ g dm^{-3}; electrolyte circulation rate: 0.11 dm^3 min^{-1}; temperature: (50 ± 2) °C; fraction: (149–177) μm; time of powder removal by brush: 15 min: (**a**, **b**) $i = 1800$ A m^{-2}, apparent density: 1.122 g cm^{-3}, and (**c**, **d**) $i = 3600$ A m^{-2}, apparent density: 0.524 g cm^{-3} (Reprinted from Ref. [50] with permission from the Serbian Chemical Society)

According to Calusaru [3], the specific surface of copper powder is 500–3000 $cm^2\ g^{-1}$ depending on the electrodeposition conditions. The critical overpotential for the dendritic growth initiation in copper sulfate acid solution is about 0.30 V, and the critical overpotential for the instantaneous dendritic growth initiation, which is equal to the critical overpotential of copper powder formation, is about 0.70 V [57]. Assuming that electrodeposition is carried out at an overpotential of the instantaneous dendritic growth initiation, it can be shown with the following: using the difference in the actual deposition overpotential and the overpotential corresponding to the beginning of the plateau of the limiting diffusion density as 0.40 V, γ_s determined in the presented way as 2.7 J cm^{-2} [39, 40], and $\eta_I(Cu) = 1$, the minimum specific powder surface, S_{sp} of 500 $cm^2\ g^{-1}$ is calculated, that is in good agreement with the findings of Calusaru [3].

In this case, the number of electrons involved in the electrodeposition reaction, n, is 2, the atomic mass of Cu, M, is 63.55 g mol^{-1}, and Faraday constant, F, is 96485 A s mol^{-1}.

6.5.2 *The Apparent Density as a Function of Specific Surface and Overpotential of the Electrodeposition*

The apparent density or volumetric mass is defined as the mass per unit volume of powder [1]. It is well known that copper powders characterized with high values of specific surface exhibit low apparent density. Powder particles from the same fraction of different powders occupy approximately the same volume, but the structure of the metallic copper can be considerably different with apparent densities, as well as the different specific surfaces [42, 43]. Obviously, the more disperse the powder particles are, the smaller is the apparent density of the copper powder, and the larger is the specific surface.

Using the data of Calusaru [3], it can be established that correlation between the apparent density and the specific surface of Cu powder is:

$$\rho_{ad} = \frac{K'}{S_{sp}} \tag{6.12}$$

where K' is constant, ρ_{ad} is the apparent density, and S_{sp} is the specific surface of Cu powder. The apparent density of powder decreases exponentially with increasing the specific surface, and a constant K' can be determined from the dependence of ρ_{ad} on S_{sp} [48].

The dependence of ρ_{ad} on deposition overpotential can be easily obtained by substitution of S_{sp} from Eq. (6.11) in Eq. (6.12) as:

$$\rho_{ad} = \frac{K' \gamma_s M \eta_I(M)}{(\eta_2 - \eta_i) nF} \tag{6.13}$$

6.5.3 The Size of Representative Particle and Particle Size Distribution

As told already, a copper powder is not formed of particles of identical size and morphology; the individual particles may assume various forms and have very different surface areas for the same average size of granule [3]. As a result of this, it is not possible to relate the powder properties with the deposition process parameters and the deposition conditions, and, hence, a representative particle of the metal powder, having at least one property the same as the powder, should be determined. Obviously, a powder can then be considered as a group of identical particles.

The representative powder particle can be defined as follows: the specific surface is the common property of a metal powder and an individual powder particle. The specific surface of powder, S_{sp}, measured in cm^2g^{-1} [3], can be determined by the method available in Ref. [61]. On the other hand, the specific surface of an individual powder particle can be calculated from its known regular geometric form. Hence, a representative powder particle is that one which is characterized by the same specific surface as a powder consisting of a mixture of different particles. The specific surface of a powder particle, $S_{sp,p}$, is given by:

$$S_{sp,p} = \frac{S_{par}}{G} \tag{6.14}$$

where S_{par} and G are the surface and the mass of particle, respectively. For a spherical particle, the specific surface $S_{sp,spher}$ is then:

$$S_{sp,spher} = \frac{3}{\rho_m r_{par}} \tag{6.15}$$

where ρ_m is the density of the metal and r_{par} is the radius of the particle. The size of a representative metal powder particle, $r_{par,r}$, can be determined by substitution of S_{sp} instead of $S_{sp,spher}$ into Eq. (6.15) which after further rearrangement gives:

$$r_{par,r} = \frac{3}{\rho_m S_{sp}} \tag{6.16}$$

In this way, the size of spherical representative powder particle is related to the property of the powder which can be determined experimentally and even calculated, as already shown in Refs. [39, 40]. The above discussion is valid if the representative particle is made of compact metal.

Assuming that copper powder can be treated as being made of some homogenous material of the density which is equal to the apparent density of the powder, ρ_{ad}, Eq. (6.16) can be written as:

$$r_{\mathrm{par,r}} = \frac{3}{S_{\mathrm{sp}}\rho_{\mathrm{ad}}} \tag{6.17}$$

The shape of the particle size distribution curves can also be discussed assuming that particles are made of a compact metal [48].

The representative particle of a copper powder has the same specific surface as the powder, meaning that mass of powder should have the same surface as mass of the representative powder particles. It follows from the above fact that two equal portions of two fractions of the particles can have the same surface as the same quantity of representative powder particles. Hence,

$$S_{1,\mathrm{m}} + S_{2,\mathrm{m}} = 2S_{\mathrm{r,m}} \tag{6.18}$$

or

$$S_{\mathrm{sp1}} + S_{\mathrm{sp2}} = 2S_{\mathrm{sp}} \tag{6.19}$$

where $S_{1,\mathrm{m}}$, $S_{2,\mathrm{m}}$, and $S_{\mathrm{r,m}}$ are the surfaces of particles 1, 2, and representative ones, respectively, and S_{sp1}, S_{sp2}, and S_{sp} are the corresponding values of specific surface. Taking into account, Eqs. (6.15) and (6.19) can be rewritten in the form:

$$\frac{1}{r_{\mathrm{par},1}} + \frac{1}{r_{\mathrm{par},2}} = \frac{2}{r_{\mathrm{par,r}}} \tag{6.20}$$

where $r_{\mathrm{par},1}$ and $r_{\mathrm{par},2}$ are the radii of the particles 1 and 2 and $r_{\mathrm{par,r}}$ is the radius of the representative particle. It follows from Eq. (6.20) that:

$$r_{\mathrm{par},1} = \frac{r_{\mathrm{par},2} \cdot r_{\mathrm{par},1}}{2r_{\mathrm{par},2} - r_{\mathrm{par,r}}} \tag{6.21}$$

which is valid for $r_{\mathrm{par},2} > r_{\mathrm{par,r}}$, if

$$r_{\mathrm{par},1} < r_{\mathrm{par,r}} < r_{\mathrm{par},2} \tag{6.22}$$

Assuming that the largest fraction of particles corresponds to the representative ones, it is now possible to calculate the shape of the particle size distribution curves, which is in perfect agreement with literature data [48].

6.5.3.1 Real Systems

In real conditions, the size and shape of powder particles depend on a regime of electrolysis, a composition of solution, deposition time, cathodic material, temperature, hydrodynamic regime, *etc.*, as illustrated by Fig. 6.10.

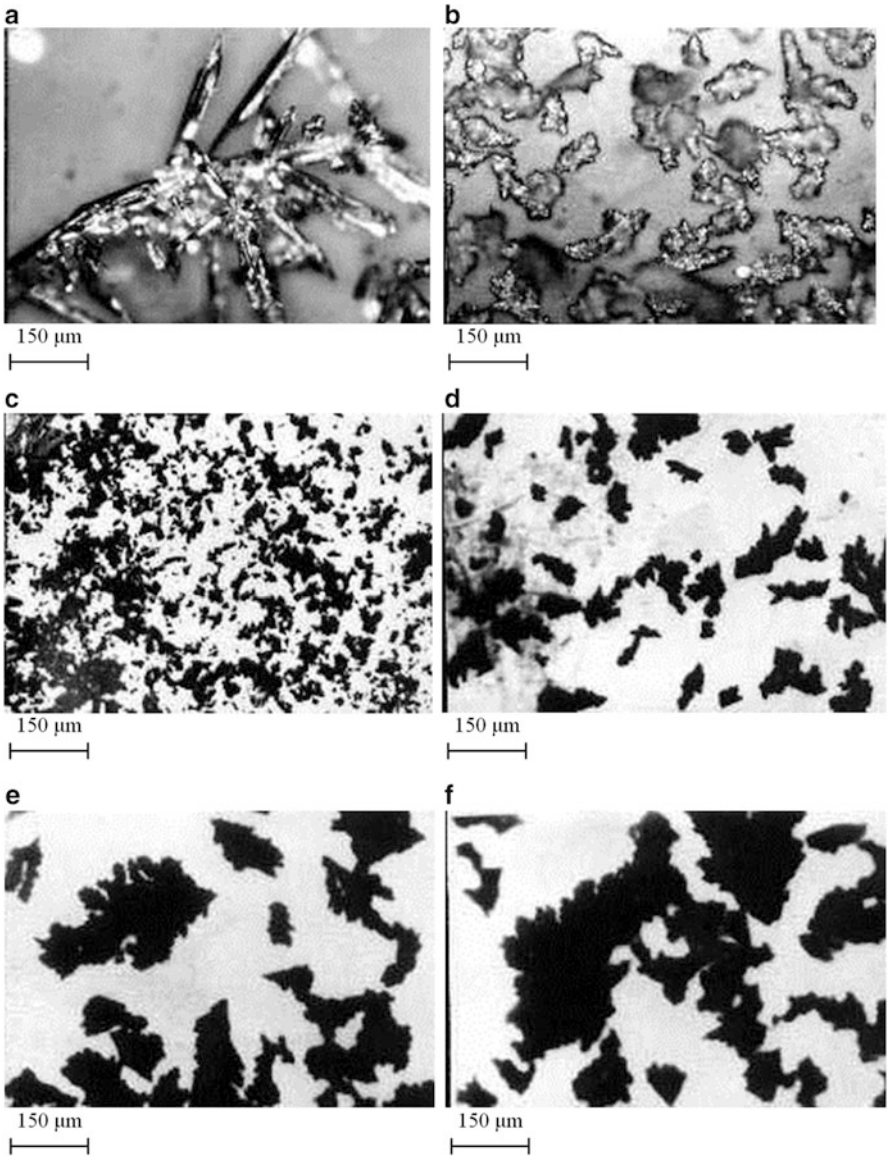

Fig. 6.10 (**a**) Silver powder particles obtained at a constant overpotential of 150 mV from 0.10 M $AgNO_3 + 0.50$ M HNO_3. Deposition time: 15 min, (**b**) silver powder particles obtained at a constant overpotential of 600 mV from 0.10 M $AgNO_3 + 0.50$ M $(NH_4)_2SO_4 + NH_4OH$ to dissolve the silver sulfate precipitate. Deposition time: 15 min. The depositions were carried out on platinum electrodes at the room temperature and copper powder particles obtained at a constant overpotential of 700 mV on Cu electrodes. Deposition time: 15 min: (**c**) 0.10 M $CuSO_4 + 0.50$ M H_2SO_4, the room temperature, (**d**) 0.10 M $CuSO_4 + 0.10$ M H_2SO_4, the room temperature, (**e**) 0.50 M $CuSO_4 + 0.50$ M H_2SO_4, the room temperature, and (**f**) 0.10 M $CuSO_4 + 0.50$ M H_2SO_4, temperature: 50 ° C (Reprinted from Ref. [5] with kind permission from Springer)

During electrodeposition of Cu at overpotentials belonging to the plateau of the limiting diffusion current density, the size and hence distribution of powder particles strongly depend on the applied overpotential of electrodeposition. The reason for it is a relatively wide range of overpotentials belonging to the plateau of the limiting diffusion current density. As already mentioned, there is no a vigorous hydrogen evolution inside this plateau. The typical particle size distribution curves for Cu powders obtained by electrodeposition at overpotentials inside (600 and 700 mV) and outside (800 mV) the plateau of the limiting diffusion current density from 0.10 M $CuSO_4$ in 0.50 M H_2SO_4 on Pt electrodes are shown in Fig. 6.11a [62]. From Fig. 6.11a, it can be seen that the increase in overpotential leads to the formation of smaller particles and to narrower particle size distribution curves.

The type of used cathodic materials had the strong effect on the shape of particle size distribution curves [6, 7, 62]. For example, at overpotentials of 600 and 700 mV (*i.e.*, at overpotentials belonging to the plateaus of the limiting diffusion current density), smaller particles and narrower distribution curves were obtained for the electrodeposition on Pt electrodes than on Al ones. This is due to fact that Al is covered with a relatively thick oxide film which causes an enlarged ohmic resistance of the electrode–solution interface of Al in relation to the one for Pt [62]. At an overpotential of 800 mV (this overpotential is outside the plateau of the limiting diffusion current density), there was no any difference in particle size distribution curves obtained on these electrodes. The reason for it is the fact that an overpotential of 800 mV is situated in the hydrogen evolution range where the process is dominantly controlled by hydrogen evolution reaction.

Anyway, increasing overpotential leads to the formation of a more disperse deposit characterized by the decreased particle size. This can be explained by the fact that increasing overpotential leads to the decrease of the height of protrusion at which dendrites start to grow instantaneously. Hence, increasing overpotential means a larger number of growth sites suitable for growth of dendrites. On the other hand [63], the velocity of dendrite growth has maximum for some optimal value of the dendrite tip radius. The optimal tip radius decreases with the increasing overpotential. With the dendrite tip radii larger than the optimal value, the difference between maximal and actual velocities of dendrite growth increases with the increasing overpotential. Hence, smaller particles and narrower particle size distribution curves are expected with the increasing overpotential of powder formation [5, 62].

The particle size distribution curves for Cu powders obtained on Pt electrodes in a galvanostatic regime at currents of 28.6, 52.0, and 133 mA are shown in Fig. 6.11b. The selected currents corresponded to average currents recorded in the potentiostatic electrodepositions at overpotentials of 600, 700, and 800 mV, respectively [62]. Formation of larger particles and less narrow distribution curves in the galvanostatic regime than those formed in the potentiostatic regime (Fig. 6.11a) can be considered as follows: during electrodeposition in the galvanostatic regime in the hydrogen evolution range, overpotential is determined by hydrogen reduction, and for the difference of overpotentials of the order 100 mV, ten times larger current of electrodeposition is required. Hence, in real

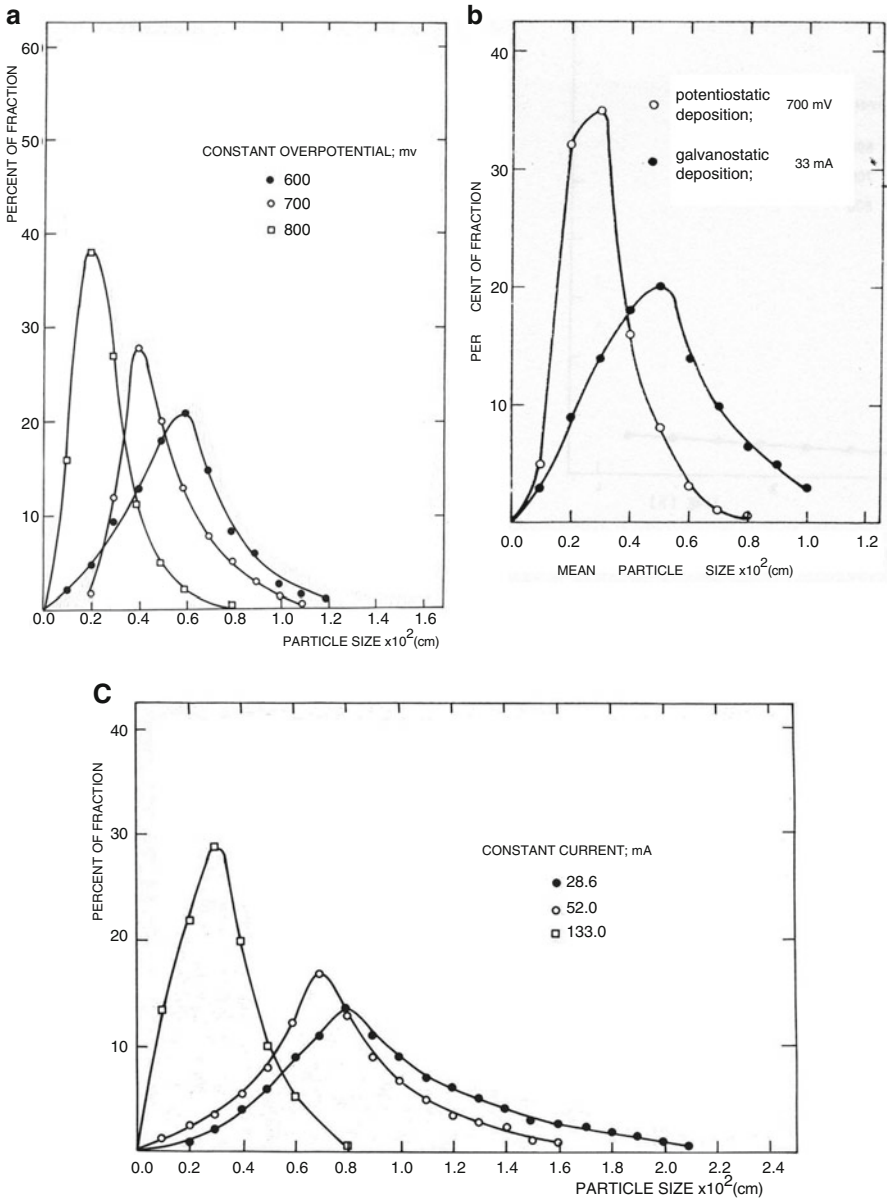

Fig. 6.11 (**a**) Particle size distribution curves for Cu powders obtained by potentiostatic electrodeposition on Pt electrodes, (**b**) particle size distribution curves for Cu powders obtained by galvanostatic electrodeposition on Pt electrodes. The surface area of the electrode: 0.63 cm^2 and (**c**) particle size distribution curves for Cu powders obtained by the potentiostatic and galvanostatic (the average current in the potentiostatic regime) electrodepositions on Cu electrodes. The surface area of the electrode: 0.63 cm^2 (Reprinted from Refs. [6, 7, 62] with kind permission from Springer)

conditions, the smaller differences in a size of the particles are expected during electrodeposition by different current densities, as well as less narrow particle size distribution curves relative to ones obtained in potentiostatic electrodeposition. The similar situation was observed when Cu was used as cathode material (Fig. 6.11c).

Anyway, the effect of the increasing current density in the galvanostatic electrodeposition is qualitative same as the increase of overpotential in potentiostatic electrodeposition, and the essence of the particle size distribution curve formation is the same in both cases.

6.5.4 *The Effect of the Particle Shape and Structure on the Flowability of Electrolytic Copper Powder*

The flowability of a copper powder depends on the interparticle friction, which is dominated by the surface area and surface roughness of the particles. As the surface area and surface roughness increase, the amount of friction in the powder mass increases and the powder exhibits less efficient flow. The same appears with the shape of particle.

The more irregular the particle shape is, the less efficient is the powder flow. Resistance to flow is the main feature of friction, which decreases as the particles approach a smooth spherical shape. The effect of particle size distribution on the powder flowability is also important. If the powder consists of monosized particles, which are more or less in point contact with one another, making the contact surface as low as possible, powdered deposits can flow. If the powder consists of different particles, the interstitial voids of the larger particles can be filled by the smaller ones, the contact surface area increases, and the flow of the powder is less efficient [1]. Hence, the best conditions for the free flow of the powder are fulfilled if the powder consists of monosized particles of spherical shape with a surface structure approaching to the structure of a smooth metal surface. This happens when the surface parts of the particles corresponding to the metal segments are larger than, or equal to, the pores between them [45], as illustrated by Fig. 6.12, and can be discussed quantitatively as follows.

It is well known that flowability of copper powders [3, 64] mainly depends on the apparent density of a copper powder. It was shown by Peissker [64] that free flow of a copper powder can be only expected if the apparent density of the powder is larger than 2.2–2.3 g cm^{-3}, while poor flow is possible at lower densities also. This can be explained in the following way. It was shown [44] that copper powder can be treated as a continuous medium, the density of which is equal to the apparent density of the powder ρ_{ad}. The density of compact metal is ρ_m. As shown in Fig. 6.13, the continuous medium can be divided into equal cubes with edge height a_c. It is obvious that spheres in the radius of which is $a_c/2$ occupy effectively the same volume and that a powder consisting of spherical particles equal to each other will be characterized by free flow. Hence, the representative particle of a copper

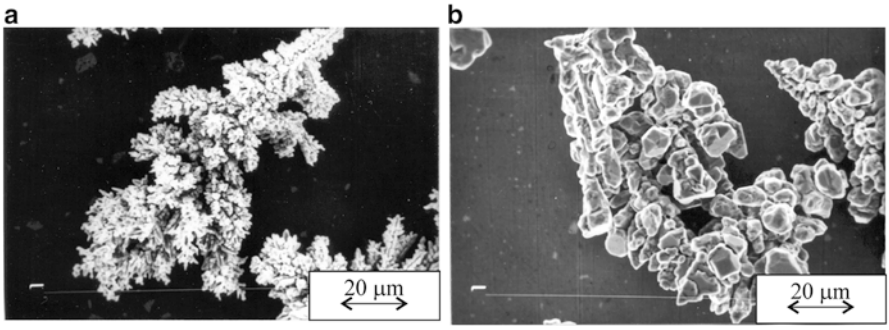

Fig. 6.12 SEM photomicrographs of Cu powder particles obtained (**a**) the constant galvanostatic regime: $i = 3600$ A m^{-2}; fraction: (149–177) μm; apparent density: 0.524 g cm^{-3}, and (**b**) the regime of reversing current: Amplitude current density: 3600 A m^{-2}; cathodic to anodic time ratio: 2.5; cathodic pulse duration: 1 s; apparent density: 1.624 g cm^{-3}. The conditions of electrolysis: $c(Cu^{2+}) = 15$ g dm^{-3}, $c(H_2SO_4) = 140$ g dm^{-3}, electrolyte circulation rate: 0.11 dm^3 min^{-1}, temperature: (50 ± 2) °C, time of powder removal by brush: 15 min (Reprinted from Ref. [7] with kind permission from Springer and Ref. [43] with permission from the Serbian Chemical Society)

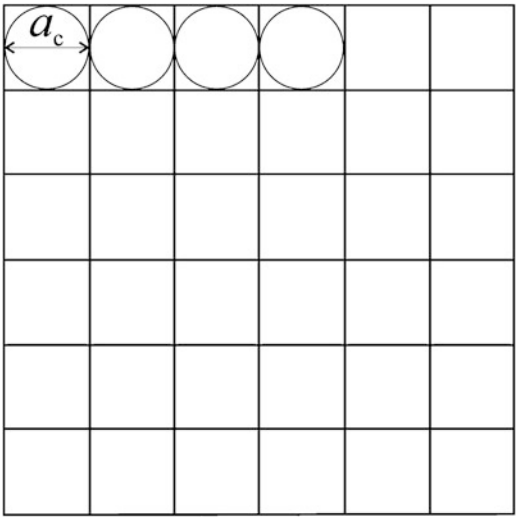

Fig. 6.13 The cross section of the part of the continuous medium divided in equal cubes and of the same volume as cubes (Reprinted from Ref. [45] with permission from the Serbian Chemical Society)

powder in respect to free flow must be spherical. The relationship between the density of the spherical representative powder particle and the apparent density of the powder can be established in the following way. It can be seen from Fig. 6.13 that instead of cubes with edge height a_c and a density ρ_{ad}, spherical particles with a radius $a_c/2$ and a density $\rho_{ad,c}$ can be considered.

Hence,

$$\frac{4}{3}\left(\frac{a_c}{2}\right)^3 \pi \rho_{ad,c} = {a_c}^3 \rho_{ad} \tag{6.23}$$

and

$$\rho_{ad,c} = \frac{6}{\pi}\rho_{ad} \tag{6.24}$$

This means that the density of the spherical particles of which a powder is composed is about twice as big as the apparent density of the powder. On the other hand, it is necessary to bear in mind that copper powder particles are dendritic by nature [42], hence they are porous. It is obvious that the free flow of a powder consisting of spherical particles can be expected only if the surface parts of the particles corresponding to the metal segments are larger than, or equal to, the pores between them.

Hence, the critical density of a particle itself $\rho_{ad,c}$ is then given by:

$$\rho_{ad,c} = \frac{1}{2}\rho_m \tag{6.25}$$

or taking into account Eq. (6.24) after further rearranging one obtains:

$$\rho_{ad} = \frac{\pi}{12}\rho_m \tag{6.26}$$

Using $\rho_m = 8.9$ g cm^{-3} for Cu, it follows from Eq. (6.26) that the critical value of the apparent density resulting in free flow of copper powder is 2.32 g cm^{-3}. This is in good agreement with the findings of Peisseker [64] for non-sieved copper powders.

References

1. German RM (1994) Powder metallurgy science, 2nd edn. Metal Powder Industries Federation, Princeton
2. Pavlović MG, Popov KI (2005) Electrochem encyclopedia. http://electrochem.cwru.edu/ed/encycl/
3. Calusaru A (1979) Electrodeposition of metal powders, Materials science monographs. Elsevier, New York
4. Orhan G, Hapci G (2010) Effect of electrolysis parameters on the morphologies of copper powder obtained in a rotating cylinder electrode cell. Powder Technol 201:57–63
5. Popov KI, Djokić SS, Grgur BN (2002) Fundamental aspects of electrometallurgy. Kluwer Academic/Plenum Publishers, New York
6. Popov KI, Pavlović MG (1993) Electrodeposition of metal powders with controlled grain size and morphology. In: White RE, Bockris JO'M, Conway BE (eds) Modern aspects of electrochemistry, vol 24. Plenum Press, New York, pp 299–391

7. Nikolić ND, Popov KI (2012) Electrodeposition of copper powders and their properties. In: Djokić SS (ed) Electrochemical production of metal powders, vol 54, Series: modern aspects of electrochemistry. Springer, New York, pp 125–185
8. Ibl N (1962) Advances in electrochemistry and electrochemical engineering, vol 2. Interscience, New York
9. Winand R (1994) Electrodeposition of metals and alloys – new results and perspectives. Electrochim Acta 39:1091–1105
10. Kozlov VM, Peraldo Bicelli L (1999) Influence of the nature of metals on the formation of the deposit's polycrystalline structure during electrocrystallization. J Cryst Growth 203:255–260
11. Nikolić ND, Popov KI (2014) A new approach to the understanding of the mechanism of lead electrodeposition. In: Djokić SS (ed) Electrodeposition and surface finishing, vol 57, Series: modern aspects of electrochemistry. Springer, New York, pp 85–132
12. Jović VD, Nikolić ND, Lačnjevac UČ, Jović BM, Popov KI (2012) Morphology of different electrodeposited pure metal powders. In: Djokić SS (ed) Electrochemical production of metal powders, vol 54, Series: modern aspects of electrochemistry. Springer, New York, pp 63–123
13. Popov KI, Krstajić NV, Čekerevac MI (1996) The mechanism of formation of coarse and disperse electrodeposits. In: White RE, Conway BE, Bockris JO'M (eds) Modern aspects of electrochemistry, vol 30. Plenum Press, New York, pp 261–312
14. Nikolić ND, Vaštag DjDj, Živković PM, Jokić B, Branković G (2013) Influence of the complex formation on the morphology of lead powder particles produced by the electrodeposition processes. Adv Powder Technol 24:674–682
15. Djokić SS, Nikolić ND, Živković PM, Popov KI, Djokić NS (2011) Electroless deposition and electrodeposition of metallic powders: a comparison. ECS Trans 33:7–31
16. Wranglen G (1960) Dendrites and growth layers in the electrocrystallization of metals. Electrochim Acta 2:130–146
17. Liaw HM, Faust JW Jr (1973) Effect of growth parameters on habit and morphology of electrodeposited lead dendrites. J Cryst Growth 18:250–256
18. Nikolić ND, Maksimović VM, Branković G, Živković PM, Pavlović MG (2013) Influence of the type of electrolyte on morphological and crystallographic characteristics of lead powder particles. J Serb Chem Soc 78:1387–1395
19. Popov KI, Čekerevac MI (1989) Dendritic electrocrystallization of cadmium from acid sulphate solution. II. The effect of the geometry of dendrite precursors on the shape of dendrites. Surf Coat Technol 37:435–440
20. Nikolić ND, Živković PM, Jokić B, Pavlović MG, Stevanović JS (2014) Comparative analysis of the polarisation and morphological characteristics of electrochemically produced powder forms of the intermediate metals. Maced J Chem Chem Eng 33:169–180
21. Lv Z-Y, Li A-Q, Fei Y, Li Z, Chen J-R, Wang A-J, Feng J-J (2013) Facile and controlled electrochemical route to three-dimensional hierarchical dendritic gold nanostructures. Electrochim Acta 109:136–144
22. Han J, Liu J (2012) Electrodeposition of crystalline dendritic silver in 12-tungstosilicate acid system. J Nanoeng Nanomanuf 2:171–174
23. Mandke MV, Han S-H, Pathan HM (2012) Growth of silver dendritic nanostructures via electrochemical route. CrystEngComm 14:86–89
24. Nikolić ND, Pavlović LjJ, Pavlović MG, Popov KI (2008) Morphologies of electrochemically formed copper powder particles and their dependence on the quantity of evolved hydrogen. Powder Technol 185:195–201
25. Nikolić ND, Popov KI (2010) Hydrogen co-deposition effects on the structure of electrodeposited copper. In: Djokić SS (ed) Electrodeposition: theory and practice, vol 48, Series: modern aspects of electrochemistry. Springer, New York, pp 1–70
26. Jović VD, Jović BM, Maksimović VM, Pavlović MG (2007) Electrodeposition and morphology of Ni, Co and Ni–Co alloy powders: part II. Ammonium chloride supporting electrolyte. Electrochim Acta 52:4254–4263

27. Lačnjevac UČ, Jović BM, Jović VD (2009) Morphology and composition of the Fe–Ni powders electrodeposited from citrate containing electrolytes. Electrochim Acta 55:535–543
28. Maksimović VM, Nikolić ND, Kusigerski VB, Blanuša JL (2015) Correlation between morphology and magnetic properties of electrochemically produced cobalt powder particles. J Serb Chem Soc 80:197–207
29. Jović VD, Maksimović VM, Pavlović MG, Popov KI (2006) Morphology, internal structure and growth mechanism of electrodeposited Ni and Co powders. J Solid State Electrochem 10:373–379
30. Jović VD, Jović BM, Pavlović MG (2006) Electrodeposition of Ni, Co and Ni–Co alloy powders. Electrochim Acta 51:5468–5477
31. Nikolić ND, Branković G, Lačnjevac U (2012) Formation of two-dimensional (2D) lead dendrites by application of different regimes of electrolysis. J Solid State Electrochem 16:2121–2126
32. Lowenheim FA (1978) Electroplating. McGraw-Hill Book Company, New York/St. Louis
33. Nikolić ND, Pavlović LjJ, Krstić SB, Pavlović MG, Popov KI (2008) Influence of ionic equilibrium in the $CuSO_4$-H_2SO_4-H_2O system on the formation of irregular electrodeposits of copper. Chem Eng Sci 63:2824–2828
34. Nikolić ND, Pavlović LjJ, Branković G, Pavlović MG, Popov KI (2008) The ionic equilibrium in the $CuSO_4$-H_2SO_4-H_2O system and the formation of the honeycomb-like structure during copper electrodeposition. J Serb Chem Soc 73:753–760
35. Nikolić ND, Popov KI, Pavlović LjJ, Pavlović MG (2006) The effect of hydrogen codeposition on the morphology of copper electrodeposits. I. The concept of effective overpotential. J Electroanal Chem 588:88–98
36. Nikolić ND, Branković G, Pavlović MG (2012) Correlate between morphology of powder particles obtained by the different regimes of electrolysis and the quantity of evolved hydrogen. Powder Technol 221:271–277
37. Nikolić ND, Branković G (2010) Effect of parameters of square-wave pulsating current on copper electrodeposition in the hydrogen co-deposition range. Electrochem Commun 12:740–744
38. Popov KI, Stojilković ER, Radmilović V, Pavlović MG (1997) Morphology of lead dendrites electrodeposited by square-wave pulsating overpotential. Powder Technol 93:55–61
39. Popov KI, Nikolić ND, Rakočević Z (2002) An estimation of the interfacial energy of the copper-copper sulphate solution interface and of the specific surface of copper powder. J Serb Chem Soc 67:635–638
40. Popov KI, Nikolić ND, Rakočević Z (2002) The estimation of solid copper surface tension in copper sulfate solutions. J Serb Chem Soc 67:769–775
41. Nikolić ND, Krstić SB, Pavlović LjJ, Pavlović MG, Popov KI (2008) The mutual relation of decisive characteristics of electrolytic copper powder and effect of deposition conditions on them. In: Hayashi K (ed) Electroanalytical chemistry research trends. NOVA Publishers, New York, pp 185–209
42. Pavlović MG, Pavlović LjJ, Ivanović ER, Radmilović V, Popov KI (2001) The effect of particle structure on apparent density of electrolytic copper powder. J Serb Chem Soc 66:923–933
43. Popov KI, Pavlović LjJ, Ivanović ER, Radmilović V, Pavlović MG (2002) The effect of reversing current deposition on the apparent density of electrolytic copper powder. J Serb Chem Soc 67:61–67
44. Popov KI, Nikolić ND, Rakočević Z (2002) A representative particle of copper powder and branching of copper dendrites. J Serb Chem Soc 67:861–866
45. Popov KI, Krstić SB, Pavlović MG (2003) The critical apparent density for the free flow of copper powder. J Serb Chem Soc 68:511–513
46. Popov KI, Krstić SB, Obradović MČ, Pavlović MG, Pavlović LjJ, Ivanović ER (2003) The effect of the particle shape and structure on the flamability of copper powder I. Modelling of a representative powder particle. J Serb Chem Soc 68:771–777

47. Popov KI, Pavlović MG, Pavlović LjJ, Ivanović ER, Krstić SB, Obradović MČ (2003) The effect of the particle shape and structure on the flowability of copper powder II. The experimental verification of the model of the representative powder particle. J Serb Chem Soc 68:779–783
48. Popov KI, Živković PM, Krstić SB (2003) The apparent current density as a function of the specific surface of copper powder and the shape of the particle size distribution curve. J Serb Chem Soc 68:903–907
49. Popov KI, Krstić SB, Obradović MČ, Pavlović MG, Pavlović LjJ, Ivanović ER (2004) The effect of the particle shape and structure on the flamability of electrolytic copper powder III. A model of the surface of a representative particle of flowing copper powder electrodeposited by reversing current. J Serb Chem Soc 69:43–51
50. Popov KI, Krstić SB, Pavlović MG, Pavlović LjJ, Maksimović VM (2004) The effect of the particle shape and structure on the flamability of electrolytic copper powder. IV. The internal structure of the powder particles. J Serb Chem Soc 69:817–825
51. Popov KI, Nikolić ND, Krstić SB, Pavlović MG (2006) Physical modelling of representative copper powder particles. J Serb Chem Soc 71:397–400
52. Nikolić ND, Popov KI, Pavlović LjJ, Pavlović MG (2007) New method of the determination of specific surface of copper obtained by the electrodeposition. Mater Prot 48:3–8
53. Pavlović MG, Nikolić ND, Popov KI (2003) The current efficiency during the cathodic period of reversing current in copper powder deposition and the overall current efficiency. J Serb Chem Soc 68:649–656
54. Pavlović MG, Pavlović LjJ, Doroslovački ID, Nikolić ND (2004) The effect of benzoic acid on the corrosion and stabilisation of electrodeposited copper powder. Hydrometallurgy 73:155–162
55. Popov KI, Pavlović LjJ, Pavlović MG, Čekerevac MI (1988) Electrode surface coarsening in potentiosttic copper electrodeposition. Surf Coat Technol 35:39–45
56. Popov KI, Pavlović MG, Pavlović LjJ, Čekerevac MI, Remović GŽ (1988) Electrode surface coarsening in pulsating overpotential copper electrodeposition. Surf Coat Technol 34:355–363
57. Popov KI, Maksimović MD, Trnjančev JD, Pavlović MG (1981) Dendritic electrocrystallization and the mechanism of powder formation in the potentiostatic electrodeposition of metals. J Appl Electrochem 11:239–246
58. Popov KI, Maksimović MD, Pavlović MG, Lukić DT (1980) The mechanism of copper powder formation in potentiostatic deposition. J Appl Electrochem 10:299–308
59. Despić AR, Popov KI (1972) Transport controlled deposition and dissolution of metals. In: Conway BE, Bockris JO'M (eds) Modern aspects of electrochemistry, vol 7. Plenum Press, New York, pp 199–313
60. Nikolić ND, Rakočević Z, Popov KI (2005) Nanostructural analysis of bright metal surfaces in relation to their reflectivities. In: Conway BE, Vayenas CG, White RE, Gamboa-Adelco ME (eds) Modern aspects of electrochemistry, vol 38. Kluwer Academic/Plenum Publishers, New York, pp 425–474
61. Schatt W, Wierters KP (1997) Powder metallurgy – processing and materials. European Powder Metallurgy Association, Technical University Dresden, Shrewsbury
62. Popov KI, Pavlović MG, Maksimović MD, Krstajić SS (1978) The comparison of galvanostatic and potentiostatic copper powder deposition on platinum and aluminium electrodes. J Appl Electrochem 8:503–514
63. Barton JL, Bockris JO'M (1962) The electrolytic growth of dendrites from ionic solutions. Proc Roy Soc A268:485–505
64. Peissker E (1984) Production and properties of electrolytic copper powder. Int J Powder Metallurgy Powder Technol 20:87–102